Applied Ocean Research 65 (2017) 327–337

Contents lists available at ScienceDirect

Applied Ocean Research

journal homepage: www.elsevier.com/locate/apor

Benchmark computations of wave run-up on single cylinder and four cylinders by naoe-FOAM-SJTU solver

Hongjian Cao, Decheng Wan*

State Key Laboratory of Ocean Engineering, School of Naval Architecture, Ocean and Civil Engineering, Shanghai Jiao Tong University, Collaborative Innovation Center for Advanced Ship and Deep-Sea Exploration, Shanghai 200240, China

ARTICLE INFO

Article history:
Received 26 January 2015
Received in revised form 12 August 2016
Accepted 30 October 2016
Available online 4 February 2017

Keywords:
Wave run-up
Cylinders
Naoe-FOAM-SJTU solver
Numerical wave tank
Benchmark computations

ABSTRACT

The benchmark simulations of wave run-up on a fixed single truncated circular cylinder and four circular cylinders are presented in this paper. Our in-house CFD solver naoe-FOAM-SJTU is adopted which is an unsteady two-phase CFD code based on the open source package OpenFOAM. The Navier-Stokes equations are employed as the governing equations, and the volume of fluid (VOF) method is applied for capturing the free surface. Monochromatic incident waves with the specified wave period and wave height are simulated and wave run-up heights around the cylinder are computed and recorded with numerical virtual wave probes. The relationship between the wave run-up heights and the incident wave parameters are analyzed. The numerical results indicate that the presented naoe-FOAM-SJTU solver can provide accurate predictions for the wave run-up on one fixed cylinder and four cylinders, which has been proved by the comparison of simulated results with experimental data.

1. Introduction

Wave run-up is the phenomenon of wave uprush on large vertical supporting cylinders of offshore structures. Wave run-up height is defined as the maximum vertical wave elevation to the still water surface, which is considerable larger than the incident wave crest especially in steep waves. It is a very important factor for the design of a safe deck elevation if large loads of wave impact on deck are to be avoided. Wave run-up generally occurs along with the strongly nonlinear phenomena such as wave impact, wave turning over and even wave breaking and spray. All these factors lead to the difficulty of accurately predicting the wave run-up value. Development of an effective and accurate numerical tool for the prediction of wave run-up and wave impact loads on supporting cylinders is both necessary and inevitable for the optimal design of offshore structures.

Numerous experimental and numerical investigations on wave run-up on a single vertical cylinder have been reported over the last several decades. In the early days, the approximate results of maximum wave run-up on a single cylinder according to linear diffraction theory proposed by MacCamy and Fuchs [1] are given as

$$\frac{R}{\eta_{\max}} = \left[1 + 4(ka)^2\right]^{1/2} \tag{1}$$

where $\eta_{\max}$ denotes the incident wave crest elevation; k denotes the wavenumber; a denotes the radius of the circular cylinder. However, the linear diffraction method is not sufficient for predicting wave run-up accurately. Therefore, the second order diffraction theory was applied for the wave run-up calculation by Kriebel [2] and compared with his experiments, but the numerical results of wave run-up were still under-predicted especially for steep waves.

Proposing empirical formula based on experimental work is another way to predict wave run-up height. The first notable experiment of wave run-up on cylinders was conducted by Hallermeier [3], and the velocity stagnation head method was suggested for calculating the wave run-up height, which was given as

$$R = \eta_{\max} + \frac{u^2}{2g} \tag{2}$$

where u denotes the horizontal velocity of water particles. This method can give reasonable results for long waves. In addition, a series of experimental work on wave run-up problems was also performed by Niedzwecki and Duggal [4], Martin et al. [5], Mase et al. [6], Nielsen [7], Morris-Thomas [8], Morris-Thomas and Thi-

* Corresponding author.
E-mail addresses: dcwan@sjtu.edu.cn, wan.decheng@126.com (D. Wan).

http://dx.doi.org/10.1016/j.apor.2016.10.011
0141-1187/

agarajan [9], De Vos et al. [10], Myrhaug and Holmedal [11], Lykke Andersen et al. [12], Ramirez et al. [13].

The rapid advance of computational fluid dynamics (CFD) technology during the last several decades has deeply affected the offshore structure design process. CFD simulation has become an efficient tool for the investigation and superior understanding of the complex physical phenomena. Numerous previous numerical simulations have also been performed on wave run-up problems. Yang & Ertekin [14] studied the nonlinear wave diffraction by a vertical cylinder numerically. Buchmann et al. [15] used the second-order boundary element model for the wave run-up problem. Trulsen and Teigen [16] applied the fully nonlinear potential method for computing the wave scattering around a vertical cylinder. Kristiansen et al. [17] performed a validation of second-order analysis approach for the prediction of diffracted wave elevation around a vertical cylinder. Sheikh and Swan [18] investigated the interaction between steep waves and vertical surface-piercing column. Lee et al. [19] simulated the wave run-up on a vertical cylinder by a 3-dimensional VOF method based on a two-step projection algorithm, and discussed the nonlinear wave-cylinder interaction. Danmeier et al. [20] compared the wave run-up results from the second-order diffraction code (WAMIT) and the fully nonlinear CFD program (ComFLOW) with experiments. The regular wave run-up on a single cylinder was also carried out numerically in the previous work. Cao and Wan [21] showed that the obtained results of wave run-up was reasonable but not accurate enough especially under steep waves when compared with those from Nielsen [7], as linear wave was used as the incident wave condition.

Investigation of wave run-up on multiple cylinders is also extremely important especially for the design of an offshore platform supported by multiple columns. Previously, many experiments were carried out to study the wave run-up on the platform columns. Niedzwecki and Huston [22] studied the wave run-up on a four-column TLP in regular wave conditions. Nielsen [7] investigated the air-gap and wave run-up on a four-column floating platform. Mavrakos et al. [23] analyzed the wave run-up on a scaled TLP model experimentally. Contento et al. [24] studied the wave run-up on an array of vertical cylinders and showed the occurrence of the second-order near trapping phenomena. Simos et al. [25] performed a series of tests for small-scale columns under regular waves, focusing on the air gap response. Izadparast and Niedzwecki [26] studied the distributions of wave run-up on a TLP model with a developed three-parameter distribution model. All the work shows the significance of investigating the wave run-up phenomena. Meanwhile, numerous numerical investigations have been conducted on the interaction between wave and multiple cylinders. Ma et al. [27] investigated the full nonlinear interaction between vertical cylinders and steep waves with finite element method. Stansberg & Kristiansen [28] investigated the nonlinear wave-column interaction in steep waves with second-order numerical model. Wang & Wu [29] studied the fully nonlinear interactions between water waves and vertical cylinder arrays based on finite element method. Bai et al. [30] studied the wave diffraction around an array of fixed vertical cylinder, and investigated the nonlinear properties of the near-trapping phenomenon associated with multiple cylinders. The investigations both with experiments and numerical models indicated that there is an urgent demand for a more efficient and accurate solver for the wave run-up prediction.

The objective of the paper is to apply the in-house CFD solver naoe-FOAM-SJTU to the benchmark computation of wave run-up on a single cylinder and multiple cylinders, considering the strongly nonlinear effects under extremely large and steep waves. All the simulations are performed in a full-scale numerical wave tank established by the numerical wave tank module of naoe-FOAM-SJTU solver. The solver is an unsteady two-phase viscous fluids flow solver employing Navier-Stokes equations as the governing equations and the volume of fluid (VOF) method for capturing the free surface. More details about naoe-FOAM-SJTU solver can refer to references [31–38]. By comparing the numerical results with corresponding experimental data, the accuracy of present solver is validated and more detailed flow field information is presented to have a deeper insight into the wave run-up phenomena.

This paper is organized as follows: the research work on the wave run-up on cylinders is reviewed firstly. The numerical methods proposed in the presented work are introduced in next section. Then, numerical simulations are performed and results of the wave run-up height around the cylinder are analyzed and discussed. Finally, a brief conclusion is drawn.

2. Numerical methods

2.1. Governing equations

Both air and water are assumed as incompressible viscous fluids. The Navier-Stokes equations are employed as the governing equations as follows:

$$\nabla \cdot \vec{u} = 0 \tag{3}$$

$$\frac{\partial}{\partial t}(\rho\vec{u}) + \nabla \cdot (\rho\vec{u}\vec{u}) - \nabla \cdot \left(\mu \left(\nabla\vec{u} + \nabla\vec{u}^T\right)\right) = -\nabla p + \rho\vec{g} + \vec{F}_S \tag{4}$$

where $\vec{u}$, p, ρ, $\mu$and $\vec{g}$ denote the velocity, pressure, density, dynamic viscosity and acceleration of gravity respectively. $\vec{F}_S$ is the source term for wave damping in the wave damping zone to avoid wave reflection from the outlet boundary. The linear and quadratic formulas are often used for wave damping, and the quadratic version is expressed as follows:

$$\vec{F}_S(x) = \begin{cases} -\rho\vec{u}\mu_S\left(\dfrac{x - x_0}{l_S}\right)^2 \text{ if} x_0 < x \le (x_0 + l_S) \\ 0 \text{ if} x \le x_0 \end{cases} \tag{5}$$

where μ_S denotes a constant parameter to adjust the wave damping effect; x_0 is the start position of the wave damping zone; l_S is the length of wave damping zone.

2.2. Interface capturing approach

The VOF method with interface compression technique proposed by Ruche [39] is used for capturing the water-air interface which is determined by solving the volume fraction function. Its governing equation is as follows:

$$\frac{\partial\alpha}{\partial t} + \nabla \cdot (\alpha\vec{u}) = 0 \tag{6}$$

where α denotes the volume fraction of one fluid in a cell, which has the value$0 \le \alpha \le 1$. The iso-contour of $\alpha = 0.5$ is considered as the free surface of water. The physical properties of the fluid are calculated as the weighted averages based on the volume fraction in one cell and shown as follows:

$$\begin{cases} \rho = \alpha\rho_1 + (1 - \alpha)\rho_2 \\ \mu = \alpha\mu_1 + (1 - \alpha)\mu_2 \end{cases} \tag{7}$$

in which, ρ_1 and ρ_2 are the densities of the water and air, respectively; μ_1 and μ_2 are the dynamic viscosities of the water and air, respectively.

2.3. Discretization schemes

The finite volume method (FVM) is used for solving the governing equations including Eqs. (3), (4), (6). The computational domain is discretized into numerous cells, and the flow field variables are

stored at the collocated cell centers. The discretization schemes used for each term of the governing equations are summarized as follows: The implicit Euler scheme is applied for the discretization of time domain. The transient and source terms are discretized with the second-order central difference scheme. The TVD scheme with the limited-linear flux limiter is used specially for the convective terms in momentum equations, and the van-Leer flux limiter is used for the convective term of the volume fraction equation. The linear difference scheme is employed for the discretization of gradients. In the computational process, the PISO algorithm is used to deal with the pressure and velocity coupling.

2.4. Numerical wave generation

Two main approaches have been implemented in naoe-FOAM-SJTU solver for the generation of regular waves. The first one is modeling the movement of the piston or flap type wave-maker, and the moving-mesh technique is used to achieve this approach. The other approach is applying a fixed incident wave boundary, at which both the velocity of water particles and the position of free surface are prescribed according to corresponding wave theory. Here, the second-order Stokes wave is used at the fixed inlet wave boundary. The wave profile is expressed as follows:

$$\eta = \frac{\mathrm{H}}{2}\cos(\mathrm{kx}\text{-}\omega\mathrm{t}) + \frac{\pi \mathrm{H}^2}{8\lambda}\frac{(2+\cosh 2\mathrm{kd})\cosh \mathrm{kd}}{\sinh^3 \mathrm{kd}}\cos 2(\mathrm{kx}\text{-}\omega\mathrm{t}) \quad (8)$$

and the velocity of water particle is given as

$$\begin{cases} u = \dfrac{\pi H}{T}\dfrac{\cosh kz}{\sinh kd}\cos(kx-\omega t) + \dfrac{3}{4}\dfrac{\pi^2 H^2}{T\lambda}\dfrac{\cosh 2kz}{\sinh^4 kd}\cos 2(kx-\omega t) \\ w = \dfrac{\pi H}{T}\dfrac{\sinh kz}{\sinh kd}\sin(kx-\omega t) + \dfrac{3}{4}\dfrac{\pi^2 H^2}{T\lambda}\dfrac{\sinh 2kz}{\sinh^4 kd}\sin 2(kx-\omega t) \end{cases} \quad (9)$$

where λ, T, H, k, ω, d denote the incident wave length, wave period, wave height, wave number, angular frequency and water depth, respectively. The variable z is the vertical position of the water particle in the Cartesian coordinates with the still free surface at $z = 0$.

2.5. Wave damping

Since there is no effective boundary condition that can be applied to let the waves go through without wave reflection, the wave damping zone, also called sponge layer is employed at one end of the numerical wave tank to absorb the wave energy and damp the free surface elevation before wave reaches the outlet boundary. This is achieved by adding a source term to the momentum equation as expressed in Eq. (5).

3. Results and discussion

3.1. Computational model

As shown in Fig. 1, a rectangular computational domain is set up as the model of a numerical wave tank. The length of the tank is 4 λ; the width is 1.5 λ, and the depth is λ. Here λ still represents the incident wave length. A single truncated vertical cylinder is fixed in the center of the wave tank. The diameter of the cylinder is 16 m, and the draft of the cylinder is 24 m.

The present study focuses on the free surface elevation around the cylinders. A series of virtual wave probes are arranged to record the elevation of free surface. Fig. 2 shows the locations of the probes around the single cylinder. There are 5 probes close to the cylinder surface and another 5 probes which are 8 m away from the cylinder surface in different radial directions.

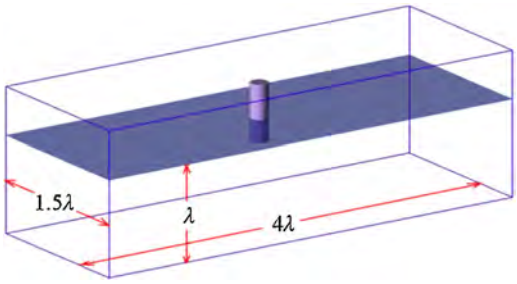

Fig. 1. The computational domain for the single cylinder.

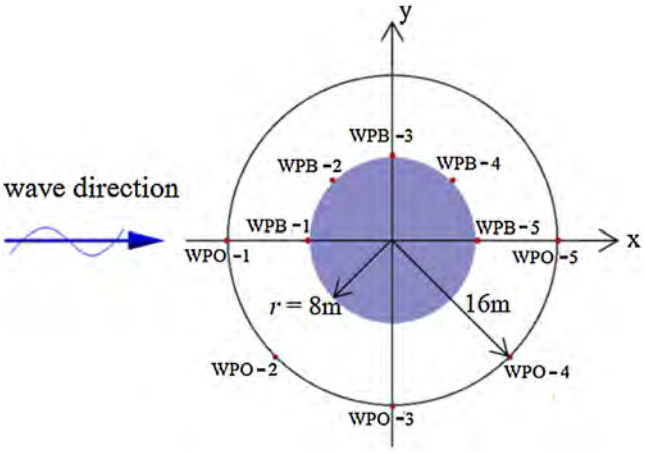

Fig. 2. The wave probe locations for the single cylinder.

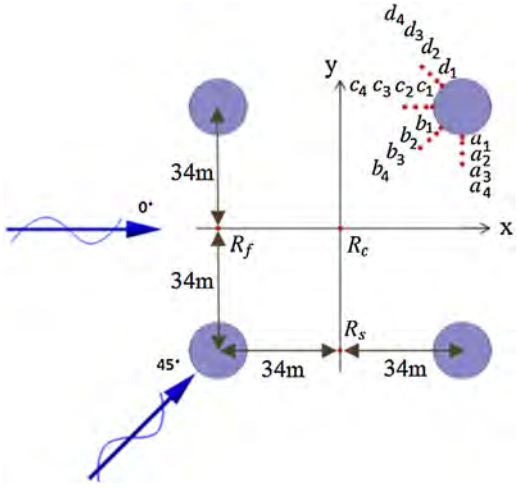

Fig. 3. The wave probe locations for the single cylinder.

For the cases of the 4-cylinder group, the width of the wave tank extends to 2 λ, and the 4 cylinders are located at the four corners of a square with a distance of 68 m between two cylinder centers. A series of wave probes is also arranged in the flow field near the cylinders. As shown in Fig. 3, there are 16 probes along 4 rows around one aft cylinder. The locations of all the probes are listed in Table 1. In addition, three other probes are also arranged at the square center R_C (0, 0), the middle point between the two front cylinders R_f (−34, 0) and the middle point between the two side cylinders R_S (0, −34). Fig. 3 also shows that two different incident wave headings are considered: θ = 0° and θ = 45°.

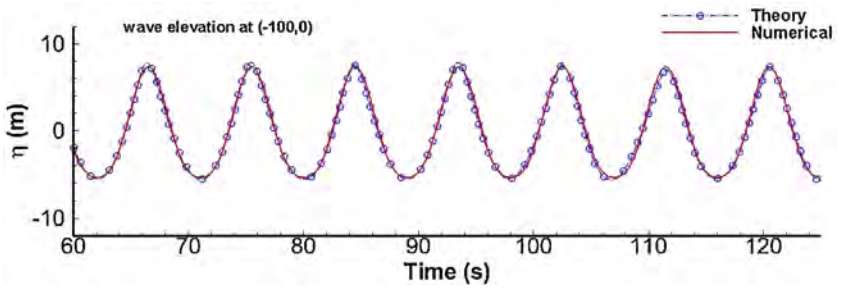

Fig. 4. Comparison of the numerical results and theory at probe (-100, 0) for T9S110.

Table 1
The wave probe locations around the aft cylinder.

Row	Radial direction	Radial distance to the center of the aft cylinder (m)			
a	270°	8.05	9.47	12.75	16.0
b	225°	8.05	9.47	12.75	16.0
c	180°	8.05	9.47	12.75	16.0
d	135°	8.05	9.47	12.75	16.0

Table 2
Wave conditions for wave Run-up cases.

H/λ	T=7s	T=9s	T=12s
1/50	T07S150	T09S150	T12S150
1/30	T07S130	T09S130	T12S130
1/16	T07S116	T09S116	T12S116
1/10	T07S110	T09S110	T12S110

3.2. Incident wave conditions

As listed in Table 2, there are totally 12 different incident wave conditions considered for the wave run-up tests on a single cylinder, including 3 different wave period values (T=7s, 9s, 12s) and 4 wave steepness values (H/λ = 1/50, 1/30, 1/16, 1/10).

For the cases of the 4-cylinder group, 3 wave steepness values (H/λ = 1/30, 1/16, 1/10) are selected for each wave period. In addition, 2 different incident wave directions ($\theta = 0^\circ$ and $\theta = 45^\circ$) are considered.

Fig. 4 shows the comparison of wave elevation between the obtained numerical results and the analytical solution with the second-order Stokes wave theory. The wave steepness is 0.10 and the wave height is 12.65 m (T9S110), which can be regarded as large steep wave. Although small differences exist at the wave crest and tough due to the higher order components, good agreement still indicates the accuracy of present solver for generating large steep waves.

The obtianed waves have the full non-linear charateristics. The harmonic components of the wave amplitude are analyzed and compared with corresponding theoretical solution, as shown in Fig. 5. The present first-order component is a bit less than theoretical value. The present second-order component is larger than the corresponding theoretical value. The theoretical third-order component is higher than second-order component. But the present thord-order component is a bit less than second-order component. For higher order components, the present numerical results agree well with the theoretical solutions. The comparisons indicate that the present numerical simulation can obtianed accurate wave condition for the wave run-up study.

Actually, the waves are generated in the numerical tank without the cylinder. The wave elevations along the wave thank are measured and compared with the theoretical solution. Fig. 6 shows the comparison between the obtained numerical results and the analytical solution of the second-order Stokes wave theory. The wave height agrees well with the theoretical solution, but the wave length become a little larger than the input wave length due to wave dispersion during the propagation. At end part of the wave tank, the wave amplitude decreases to 0 gradually due to the existence of the wave damping zone, which indicates that the wave damping zone is efficient for absorbing the wave.

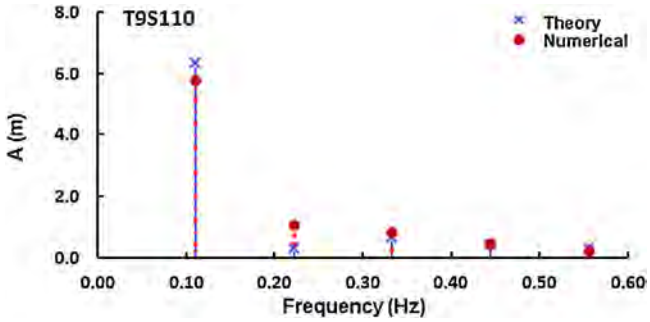

Fig. 5. Harmonic component of the wave amplitude at probe (-100, 0) for T9S110.

Table 3
Mesh Characteristics for convergence test.

	Cell counts	Grids along cylinder circle	$H/\Delta z$	$\lambda/\Delta x$	Δx_{min}, Δy_{min}
Mesh-I	0.40 million	40	10	63	0.005m
Mesh-II	0.63 million	80	10	63	0.005m
Mesh-III	0.85 million	120	10	63	0.005m
Mesh-IV	1.08 million	160	10	63	0.005m

3.3. Mesh convergence test

To further verify the efficiency and accuracy of the present solver, the mesh convergence test is carried out with 4 different meshes for the case of wave run-up on a single cylinder under the same wave condition T09S130 (T=9s, H=4.22 m). Table 3 lists the detailed information of the mesh. For the 4 different mesh configurations, the grid number along the cylinder circle increases from 40 to 160, and the corresponding cell count increases from 0.4 million to 1.08 million. In order to model the incident wave accurately and reduce the computation cost simultaneously, 10 cells are allocated in a wave height and over 60 cells in a wave length. The thickness of the first layer grids around the cylinder is 0.005 m. During the computation, the time step is adjusted automatically under the conditions that the maximum Courant Number is less than 0.5, the maximum Courant Number at the free surface is less than 0.25, and the largest time step is less than T=1/500.

The horizontal and vertical forces on the cylinder are recorded during the computation, as shown in Fig. 7. The obtained horizontal forces are the same for different meshes. The vertical forces obtained with Mesh-II, Mesh-III and Mesh-IV are the same but different from that obtained with Mesh-I, which is a bit smaller.

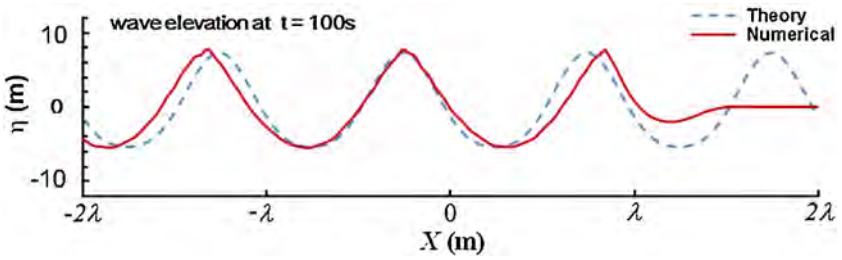

Fig. 6. Comparison of the numerical results and theory (T9S110) along the wave tank.

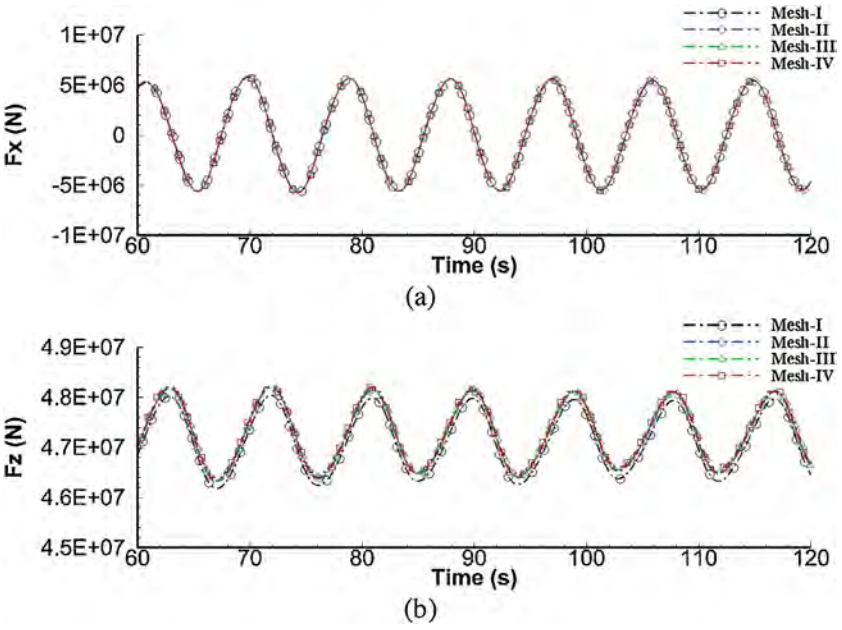

Fig. 7. Time histories of wave force on single cylinder: (a) horizontal force *Fx*; (b) vertical force *Fz*.

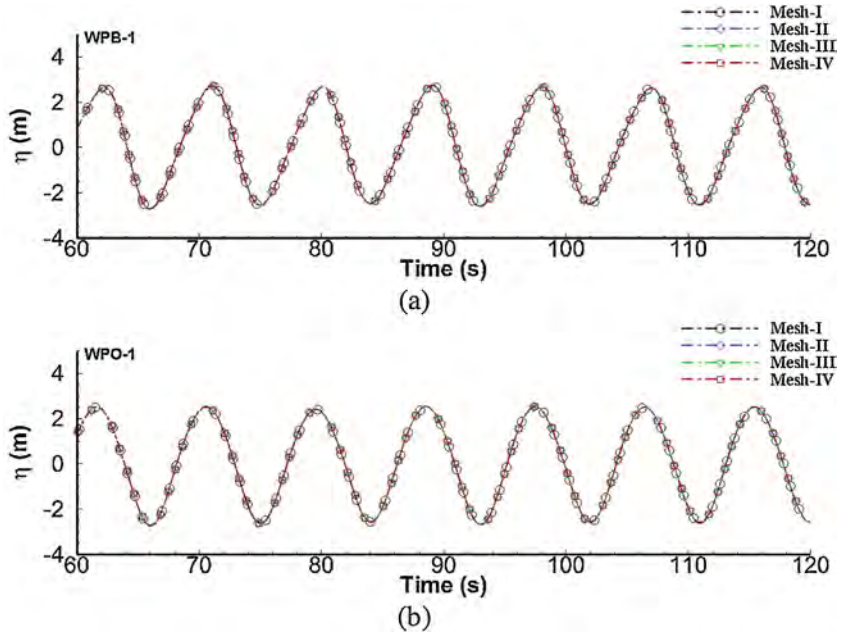

Fig. 8. Time histories of wave elevation in wave T9S130 at probes: (a) WPB-1; (b) WPO-1.

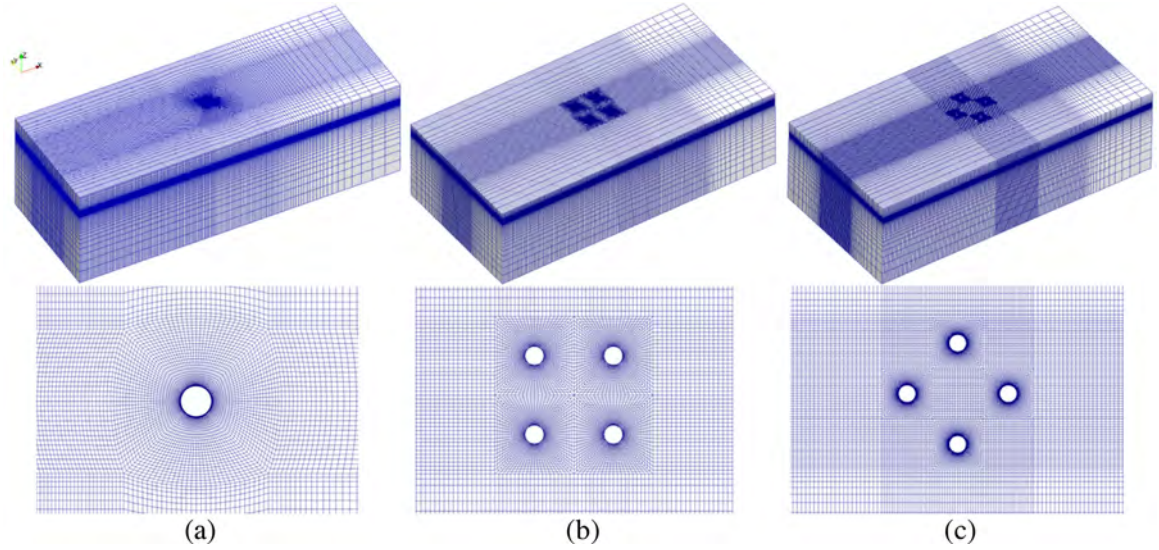

Fig. 9. Global and Local detail mesh for computations. (a) Single cylinder (b) 4-cylinder with 0° wave heading (c) 4-cylinder with 45° wave heading.

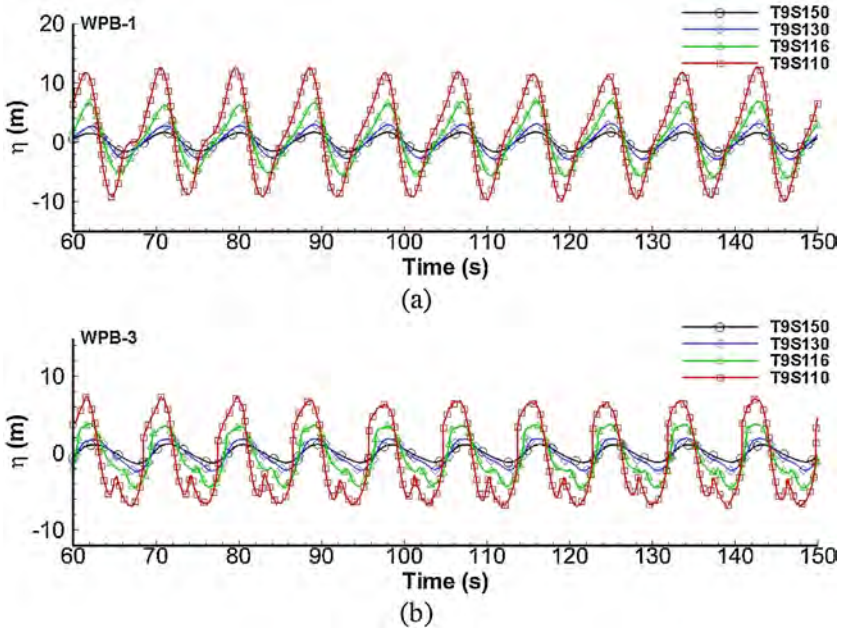

Fig. 10. Time histories of wave elevation at probes in waves (T = 9s): (a) WPB-1; (b) WPB-3.

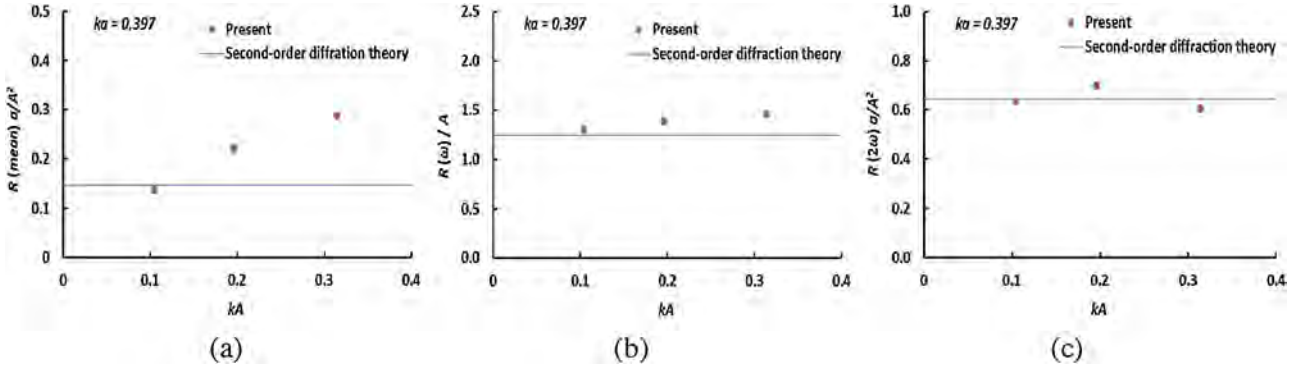

Fig. 11. Harmonic components of the wave run-up against (T = 9s): (a) mean value; (b) ω term; (c) 2ω *term.*

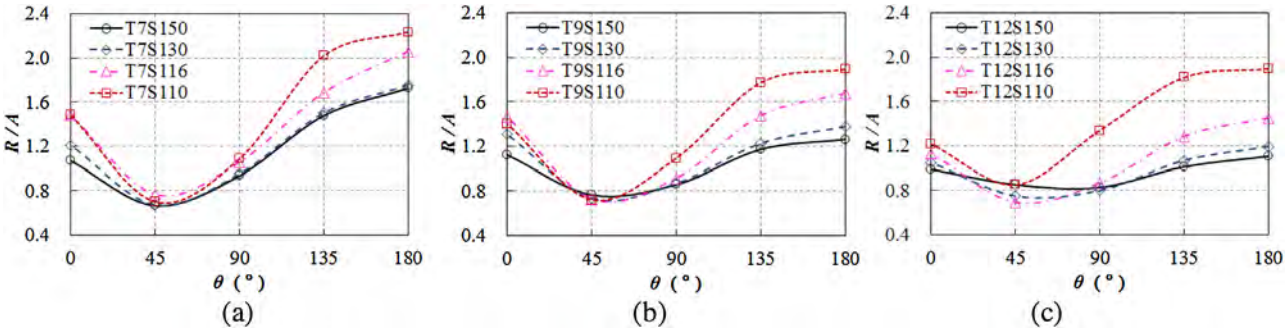

Fig. 12. Maximum wave run-up ratio at the probes close to the cylinder surface: (a) T = 7s; (b) T = 9s; (c) T = 12s.

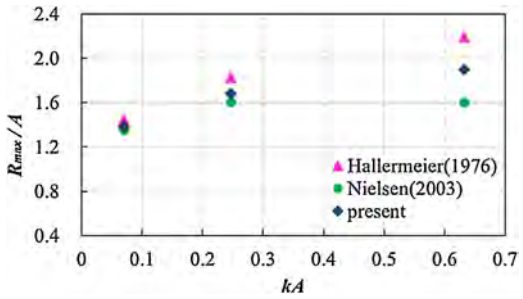

Fig. 13. Comparison of the maximum wave run-up ratio R_{max}/A.

Table 4
Wave elevation analyzed via FFT.

Probes	*Mean value*	*ω term*	*2ω term*
WPB-1	1.4402	9.2317	3.0169
WPB-2	0.4562	9.5272	1.6256
WPB-3	−0.9317	6.6529	2.2248
WPB-4	−1.1228	4.0462	1.7245
WPB-5	0.4928	6.5117	1.5191

In addition, the wave elevations at all the probes are recorded and compared. Fig. 8 shows the wave elevation at probes WPB-1 and WPO-1 obtained with the 4 different meshes. The time histories for all meshes coincide, which implies the good mesh convergence of the present solver.

Considering the computational time and resources consumed, the detailed mesh configuration of Mesh-III is used for all the other cases. The meshes used for the cases of a single cylinder and 4-cylinder group are shown in Fig. 9.

3.4. Wave run-up on a single cylinder

According to the wave conditions listed in Table 2, 12 different simulations are carried out and the wave run-up values at all the probes are recorded. Due to the paper length constraint, only the time histories of wave elevation at WPB-1 and WPB-3 with the incident wave period T = 9 s are presented, as shown in Fig. 10. It is found that the nonlinear characteristic appears more and more obvious with the increasing wave steepness. There is a series of secondary crests in the time histories of wave elevation at probe WPB-3.

The obtained time histories of wave elevation are analyzed with the Fast Fourier Transform (FFT) algorithm. The mean value, ω term and 2ω term of the wave elevation are obtained. Table 4 lists the values under wave condition T9S110. The 2ω term accounts for a large percentage, indicating the strongly nonlinear characteristic of the wave run-up phenomena.

The harmonic components of the wave run-up (mean value, ω term and 2ω *term*) are compared with corresponding results of second-order diffraction theory separately as shown in Fig. 11. The present harmonic components of wave run-up agree well with corresponding value of the second-order diffraction theory only at small wave steepness. There is much difference on all the harmonic components for large wave steepness. The mean value and ω term of wave run-up increase with the increasing wave steepness obviously.

The maximum wave run-up height at the wave probes is the most concerned, especially for the probes close to the cylinder surface. By averaging the crests values of free surface in 10 wave periods, the maximum wave run-up value at each probe is presented. Fig. 12 shows the relationship between the maximum run-up ratio R/A and the radial directional angle θ at each probe close to cylinder surface, where $A = H/2$ represents the incident wave amplitude. The maximum run-up value occurs at the head-wave side of the cylinder with the radial directional angle (θ = 180°) where the probe WPB-1 locates.

The maximum wave run-up ratio R_{max}/A at WPB-1 are calculated under different incident wave conditions as are listed in Table 5. It shows that R_{max}/A varies from 1.10 to 2.24. The largest value occurs under the condition T7S110. When the wave steepness increases, the value of R_{max}/A increases obviously. Moreover, with the same wave steepness, R_{max}/A also increases with the decreasing of wave period. In some cases with large wave steepness, R_{max}/A reaches a

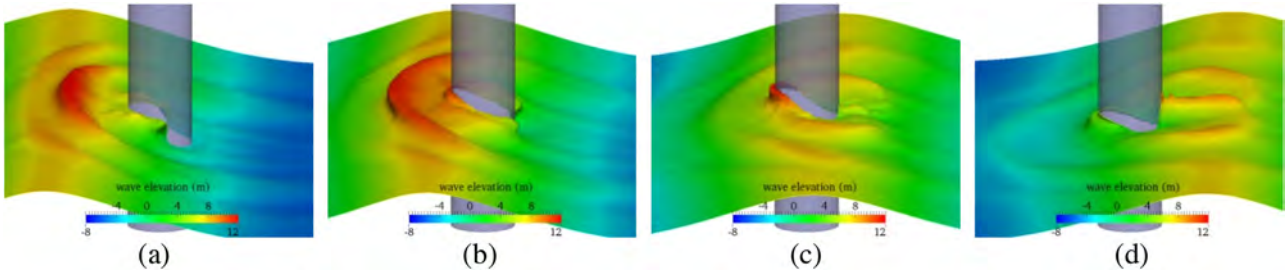

Fig. 14. Instantaneous free surface (T9S110).

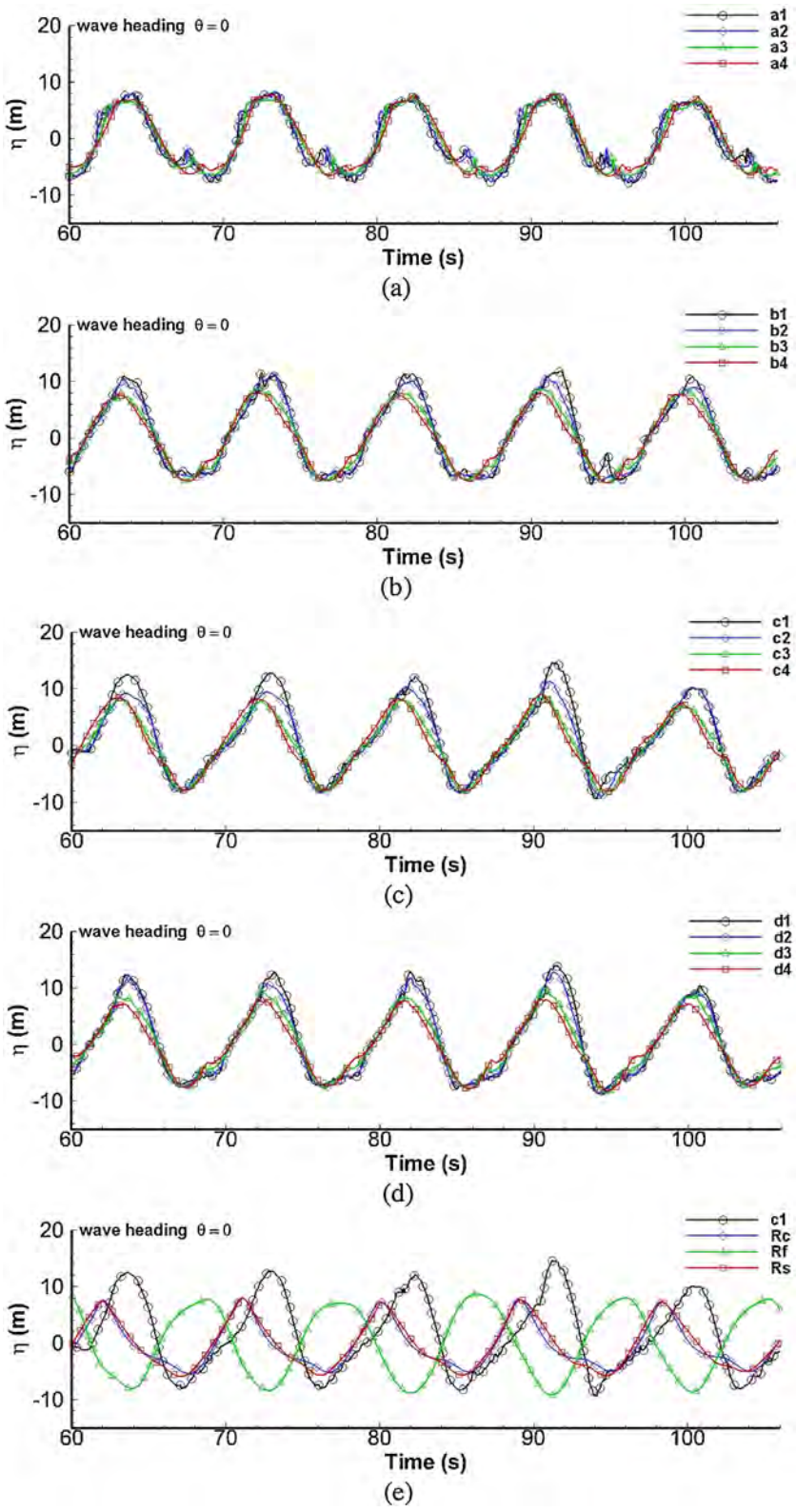

Fig. 15. Time histories of wave elevation at the probes (T9S110, θ=0°).

value larger than 2.0, especially for the conditions with wave period T = 7s.

Nielsen [7] proposed some maximum wave run-up values by experiment under the wave condition of wave period T = 9s. Fig. 13 shows the comparison of the present numerical results of maximum wave run-up ratio with the corresponding data obtained by Eqn.(2) proposed by Hallermeier [3] and the experimental data from Nielsen [7]. The present results agree well with the data from Nielsen [7], but a bit smaller than the data calculated using Eqn.(2). Good agreement implies the accuracy of the present solver for predicting the wave run-up on a single cylinder.

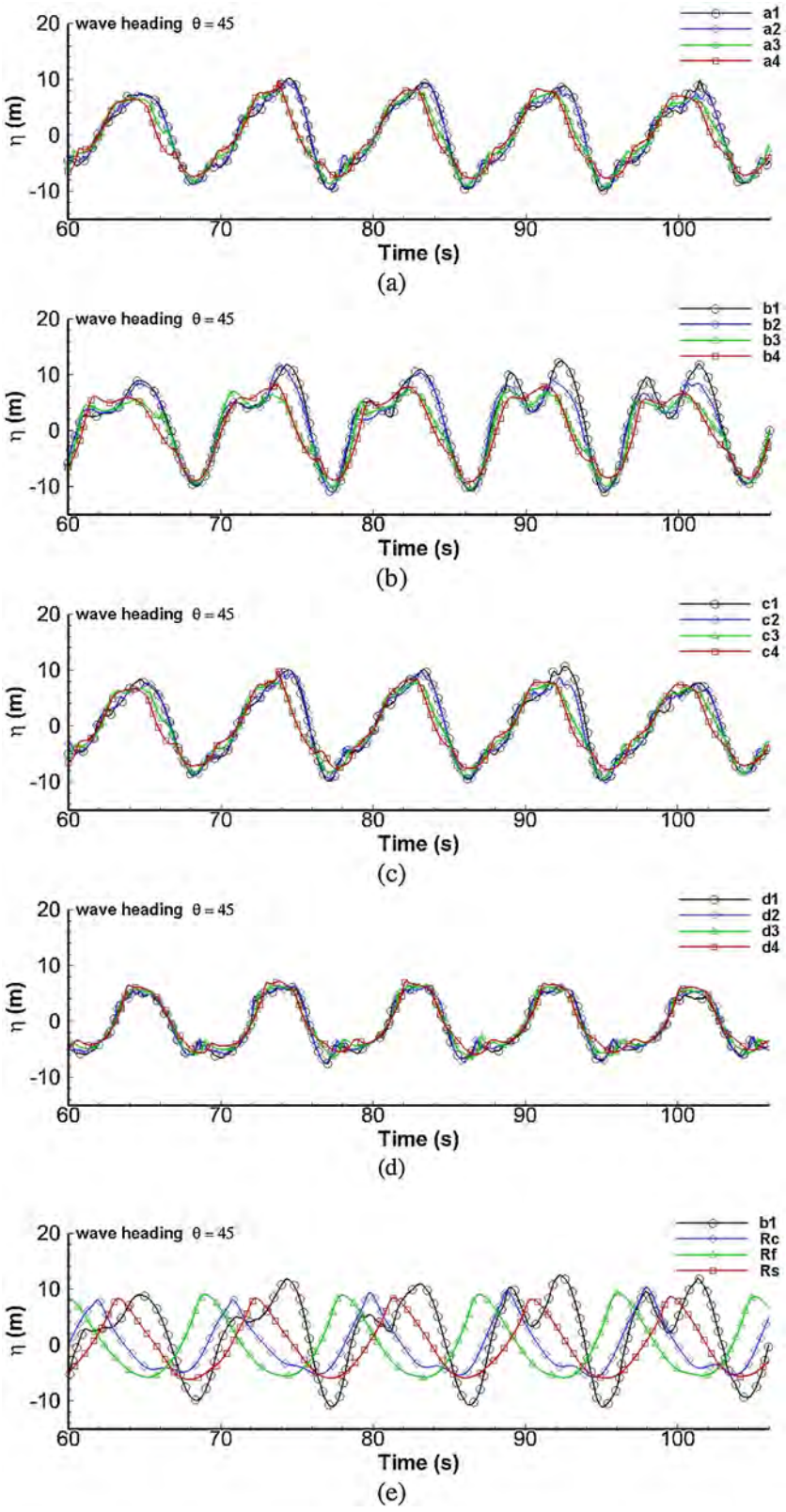

Fig. 16. Time histories of wave elevation at the probes (T9S110, θ=45°).

It is also found that the maximum run-up value at WPB-4 ($\theta = 45^\circ$) is less than that at the other probes under the same incident wave condition, especially with large wave steepness. Fig. 14 shows the instantaneous free surface near the cylinder with the incident wave T9S110. The wave diffraction field around the cylinder is obvious. The water is blocked ahead of the cylinder, and then it runs up along the cylinder resulting in the occurrence of the maxi-

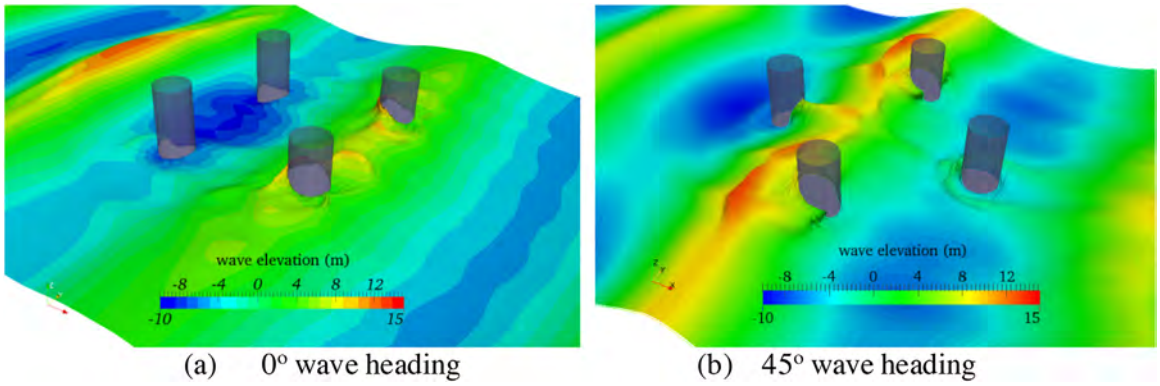

Fig. 17. Instantaneous free surface (T9S110).

Table 5
Results of maximum wave run-up ratios.

R_{max}/A	$T=7$s	$T=9$s	$T=12s$
H/λ =1/50	1.73	1.26	1.10
H/λ =1/30	1.75	1.38	1.19
H/λ =1/16	2.06	1.68	1.40
H/λ =1/10	2.24	1.89	1.90

mum wave run-up height. Besides, there is an obvious phenomenon of run-up on the rear side of the cylinder.

3.5. Wave run-up on 4-Cylinder group

For the cases of wave run-up on 4 cylinders, 9 different incident wave conditions are considered. The time histories of free surface elevation under the incident wave T9S110 with 0° and 45° wave headings are shown in Figs. 15 and 16. Due to the interference among cylinders, strong nonlinearity can be observed from the time histories of free surface elevation.

In the 0° wave heading case, the maximum wave elevation at the probes along rows *c* is larger than those along other rows. The maximum wave run-up height occurs at probe c_1. By comparing the wave elevation at c_1, R_C, R_f and R_S, it is known that the maximum wave run-up height still occurs at c_1, which is at the up-wave side of the cylinder. The wave elevation at R_f is a bit larger than that at R_C and R_S. There is not much difference between the wave elevation at R_C and R_S.

In contrast, in the case with 45° wave heading, the maximum wave run-up height on the aft cylinder is smaller than that under the 0° wave heading condition. Obviously, there are secondary troughs near the crests in the time histories of wave elevation at probes along row *b*, which is due to the strong interference among the cylinders. Similarly, the maximum wave elevations at R_C, R_f and R_S are smaller than those obtained at the probes close to the cylinder surface. The interference among the cylinders affects the distribution of the wave elevation in the area of the cylinder group and the strongly nonlinear characteristics of the free surface elevation are noticed.

Fig. 17 shows the simulated free surface around the cylinder group with different incident wave heading angles but under the same wave condition T9S110. The maximum wave elevation on the cylinder group is larger than that on a single cylinder. The obtained R_{max}/A is larger than 2.0.

4. Conclusions

The regular wave run-up on a single cylinder and four cylinders is studied numerically by using the in-house CFD solver naoe-FOAM-SJTU. The maximum wave run-up height on cylinders is of great importance and data of wave run-up can provide guidance for the design of offshore structures. By comparing the wave elevation at a series of wave probe locations, it is found that the maximum run-up height occurs at the head wave side of the cylinders. The ratio of run-up height to the wave amplitude obviously grows along with the increasing wave steepness, while the ratio decreases when the wave period or wave length becomes larger. The numerical results for the wave run-up on the 4-cylinder group show great nonlinear characteristic and indicate that the interference among the cylinders can greatly influence the wave run-up height on the cylinder group. The obtained maximum wave height is larger than that on a single cylinder. Moreover, the wave run-up on the aft cylinder with 0° wave heading is larger than that with 45° wave heading.

The present work shows that naoe-FOAM-SJTU solver has the capability of dealing with wave run-up problems with good accuracy. In the near future, this solver will be further extended to deal with more complex problems such as wave interaction with floating structures.

Acknowledgements

This work is supported by the National Natural Science Foundation of China (51379125, 51490675, 11432009, 51579145, 11272120), Chang Jiang Scholars Program (T2014099), Program for Professor of Special Appointment (Eastern Scholar) at Shanghai Institutions of Higher Learning (2013022) and Innovative Special Project of Numerical Tank of Ministry of Industry and Information Technology of China (2016-23/09), to which the authors are most grateful.

References

[1] R.C. MacCamy, R.A. Fuchs, Wave Forces on Piles: A Diffraction Theory. Tech. Memo No. 69, US Army Beach Erosion Board, Washington DC, 1954.
[2] D.L. Kriebel, Nonlinear wave interaction with a vertical circular cylinder. Part II: wave run-up, Ocean Eng. 19 (1) (1992) 75–99.
[3] R.J. Hallermeier, Nonlinear flow of wave crests past a thin pile, J. Waterw. Harbors Coastal Eng. 102 (4) (1976) 365–377.
[4] J.M. Niedzwecki, S.D. Duggal, Wave run-up and forces on cylinders in regular and random waves, J. Waterw. Port Coastal Ocean Eng. 118 (6) (1992) 615–634.
[5] A.J. Martin, W.J. Easson, T. Bruce, Run-up on columns in steep: deep water regular waves, J. Waterw. Port Coastal Ocean Eng. 127 (1) (2001) 26–32.
[6] H. Mase, K. Kosho, S. Nagahashi, Wave run-up of random waves on a small circular pier on sloping seabed, J. Waterw. Port Coastal Ocean Eng. 127 (4) (2001) 192–199.
[7] F.G. Nielsen, Comparative study on airgap under floating platforms and run-up along platform columns, Mar. Struct. 16 (1) (2003) 97–134.
[8] M.T. Morris-Thomas, Wave Run up on Vertical Columns of an Offshore Structure, The University of Western Australia, 2003.

[9] M.T. Morris-Thomas, K.P. Thiagarajan, The run-up on a cylinder in progressive surface gravity waves: harmonic components, Appl. Ocean Res. 24 (1) (2004) 98–113.
[10] L. De Vos, P. Frigaard, J. De Rouck, Wave run-up on cylindrical and cone shaped foundations for offshore wind turbines, Coastal Eng. 54 (2007) 17–29.
[11] D. Myrhaug, L.E. Holmedal, Wave run-up on slender circular cylindrical foundations for offshore wind turbines in nonlinear random waves, Coastal Eng. 57 (6) (2010) 567–574.
[12] T. Lykke Andersen, P. Frigaard, M.L. Damsgaard, L. De Vos, Wave run-up on slender piles in design conditions—model tests and design rules for offshore wind, Coastal Eng. 58 (4) (2011) 281–289.
[13] J. Ramirez, P. Frigaard, T.L. Andersen, L. de Vos, Large scale model test investigation on wave run-up in irregular waves at slender piles, Coastal Eng. 72 (1) (2013) 69–79.
[14] C. Yang, R.C. Ertekin, Numerical simulation of nonlinear wave diffraction by a vertical cylinder transactions of ASME, J. Offshore Mech. Arct. Eng. 114 (1) (1992) 36–44.
[15] B. Buchmann, J. Skourup, K.F. Cheung, Run-up on a structure due to second-order waves and a current in a numerical wave tank, Appl. Ocean Res. 20 (1998) 297–308.
[16] K. Trulsen, T. Teigen, Wave scattering around a vertical cylinder: fully nonlinear potential flow calculations compared with low order perturbation results and experiment, in: Proc 21 st Int Conf Offshore Mech and Artic Eng (OMAE), Oslo, Norway, 2002.
[17] T. Kristiansen, R. Baarholm, C.T. Stansberg, Validation of second-order analysis in predicting diffracted wave elevation around a vertical circular cylinder, in: Proceedings of the 14th International Offshore and Polar Engineering Conference, Toulon, France, 2004, pp. 342–349.
[18] R. Sheikh, C. Swan, The interaction between steep waves and a vertical, surface-piercing column, J. Offshore Mech. Arct. Eng. 127 (2005) 31–38.
[19] K.H. Lee, D.S. Kim, C.H. Kim, S.K. Lee, S.T. Kee, Wave run-up on vertical cylinder by 3-dimensional VOF method, in: Proc 17th Int Offshore and Polar Eng Conf (ISOPE), Lisbon, Portugal, 2007.
[20] D.G. Danmeier, R.K.M. Seah, T. Finnigan, D. Roddier, A. Aubault, M. Vache, J.T. Imamura, Validation of wave run-up calculation methods for a gravity based structure, in: Proc ASME 27th Int Conf Offshore Mech. and Arctic Eng (OMAE), Estoril, Portugal, 2008.
[21] H.J. Cao, D.C. Wan, Development of multidirectional nonlinear numerical wave tank by naoe-FOAM-SJTU solver, Int. J. Ocean Syst. Eng. 4 (1) (2014) 52–59.
[22] J.M. Niedzwecki, J.R. Huston, Wave interaction with tension leg platforms, Ocean Eng. 19 (1) (1992) 21–37.
[23] S.A. Mavrakos, I.K. Chatjigeorgiou, G. Grigoropoulos, Scale experiment of motions and wave run-up on a TLP model Subjected to monochromatic waves, Proc 14th Int Offshore and Polar Eng Conf (ISOPE) (2004).
[24] G. Contento, F. D'Este, M. Sicchiero, R. Codiglia, M. Calza, Run-up and wave forces on an array of vertical circular cylinders: experimental study on second-order near trapping, Int. J. Offshore Polar Eng. 15 (2) (2005) 96–103.
[25] A.N. Simos, A.L.C. Fujarra, J.V. Sparano, C.M. Umeda, R.R. Rossi, Experimental evaluation of the dynamic air gap of a large-volume semi-submersible platform, in: Proc 25 st Int Conf Offshore Mech and Artic Eng. (OMAE), Hamburg, Germany, 2006.
[26] A.H. Izadparast, J.M. Niedzwecki, Probability distributions of wave run-up on a TLP model, Mar. struct. 23 (2) (2010) 164–186.
[27] Q.W. Ma, G.X. Wu, R. Eatock Taylor, Finite element simulations of fully non-linear interaction between vertical cylinders and steep waves. Part 2: numerical results and validation, Int. J. Numer. Methods Fluids 36 (2001) 287–308.
[28] C.T. Stansberg, T. Kristiansen, Non-linear scattering of steep surface waves around vertical columns, Appl. Ocean Res. 27 (2) (2005) 65–80.
[29] C.Z. Wang, G.X. Wu, Interactions between fully nonlinear water waves and cylinders arrays in a wave tank, Ocean Eng. 37 (4) (2010) 400–417.
[30] W. Bai, X. Femh, R. Eatock Taylor, K.K. Ang, Fully nonlinear analysis of near-trapping phenomenon around an array of cylinders, Appl. Ocean Res. 44 (2014) 71–81.
[31] Z.R. Shen, D.C. Wan, An irregular wave generating approach based on naoe-FOAM-SJTU solver, China Ocean Eng. 30 (2) (2016) 177–192.
[32] D.C. Wan, Z.R. Shen, Overset-RANS computations of two surface ships moving in viscous fluids, Int. J. Comput. Methods 9 (1) (2012) 1240013 (1–14).
[33] Z.R. Shen, D.C. Wan, RANS Computations of added resistance and motions of ship in head waves, Int. J. Offshore Polar Eng. 23 (4) (2013) 263–271.
[34] Z.R. Shen, D.C. Wan, P. Carrica, Dynamic overset grids in OpenFOAM with application to KCS self-propulsion and maneuvering, Ocean Eng. 108 (2015) 287–306.
[35] Y.C. Liu, Q. Xiao, A. Incecik, D.C. Wan, Investigation of the effects of platform motion on the aerodynamics of a floating offshore wind turbine, J. Hydrodyn. 28 (1) (2016) 95–101.
[36] R.S. Zha, H.X. Ye, Z.R. Shen, D.C. Wan, Numerical computations of resistance of high speed catamaran in calm water, J. Hydrodyn. 26 (6) (2014) 930–938.
[37] Q.J. Meng, D.C. Wan, URANS simulations of complex flows around a ship entering a lock with different speeds, Int. J. Offshore Polar Eng. 26 (2) (2016) 161–168.
[38] Q.J. Meng, D.C. Wan, Numerical simulations of viscous flow around the obliquely towed KVLCC2 M model in deep and shallow water, J. Hydrodyn. 28 (3) (2016) 506–518.
[39] H. Ruche, Computional fluid dynamics of dispersed two-phase flows at high phase fractions, Imp. Coll. Sci. Technol. Med. (2002).